Charles University in Prague

Faculty of Science

Study programme: Chemistry
Branch of study: Chemistry

Peter Illés

Study of self-assembly and degree of ionization of block copolymers using transmission electron microscopy and molecular simulations

Studium samoskladby a stupně ionizace blokových kopolymerů pomocí transmisní elektronové mikroskopie a molekulových simulací

Bachelor's thesis

Supervisor: Ing. Lucie Nová PhD.

Consultant: Mgr. Michal Mazur PhD.

Prague, 2023

Prohlašuji, že jsem závěrečnou práci zpracoval samostatně a že jsem uvedl všechny použité informační zdroje a literaturu. Tato práce ani její podstatná část nebyla předložena k získání jiného nebo stejného akademického titulu.

Praha, 17. 05. 2023 Peter Illés

Abstract:
Responsive systems, such as block copolymers with solvent-affine blocks, can undergo self-assembly into structures like micelles or vesicles. These assemblies are highly sensitive to slight changes in external conditions, like pH or temperature, leading to the formation or dissolution of micelles. When one of the polymer blocks is a weak polyelectrolyte, its degree of ionization depends not only on the external conditions but also on the association state. This study focuses on investigating the size and degree of ionization of micellar structures formed by polymer chains containing thermoresponsive and pH-responsive blocks. The investigation combines high-resolution transmission electron microscopy and Hamiltonian Monte Carlo simulations to provide a comprehensive understanding of these micellar structures.

Keywords:
high resolution transmission electron microscopy; molecular simulations; self-assembly; responsive systems; block copolymers; weak polyelectrolytes

Abstrakt:
Responzivní systémy blokových kopolymerů, kterých bloky mají různou afinitu ke zkoumanému rozpouštědlu mohou vytvářet struktury jako micely nebo vezikuly. Tyhle struktury jsou senzitivní ke změnám vnějších podmínek jakými jsou pH a teplota. Tyto změny často vedou k formaci nebo rozkladu micel. Pokud je jedním z bloků slabý polyelektrolyt, stupeň ionizace závisí nejenom na vnějších podmínkách, ale taktéž na konformaci řetězců. Táto práce zahrnuje studium velikosti a stupně ionizace micelárních struktur a linearních řetězců kopolymeru obsahujícího termosenzitivní a pH responzivní bloky pomocí vysokorozlišovací transmisní elektronové mikroskopie a hamiltonianských Monte Carlo simulací.

Klíčová slova:
vysoce rozlišená transmisní elektronová mikroskopie; molekulové simulace; samoskladba; responzivní systémy; blokové kopolymery; slabé polyelektrolyty

I would like to express my gratitude to Ing. Lucie Nová, PhD., my supervisor, and Mgr. Michal Mazur, PhD., my consultant, for their invaluable guidance and unwavering support during this study and beyond. I am also grateful to doc. RNDr. Filip Uhlík, Ph.D., for providing me with simulation software and assisting me with my programming skills. Lastly, I would like to extend my thanks to my family for their undying support throughout this entire journey.

Contents

1. Introduction

Macromolecular and polymer sciences play a significant role in the research of advanced materials. The key aspect in popularity of macromolecules is their variability of properties under different sets of conditions. Due to their unique structure and properties they are widely exploited as possible drug carriers, desalination agents, tissue engineering materials [1] and much more.
Typical polymer chains are made up of repeating sections of atoms, or so called repeating units. If all of the repeating units come from a single type of monomer, we call them homopolymers. Depending on the actual structure of the repeating unit, these polymers can achieve different structures which are heavily dependent on the synthesis of the polymer.
However, if the repeating unit consists of two or more different monomers, that come from different monomers, we refer to these chains as copolymers [2]. Repeating units are often arranged into repeating patterns which are a result of both interactions between monomers and synthesis conditions.

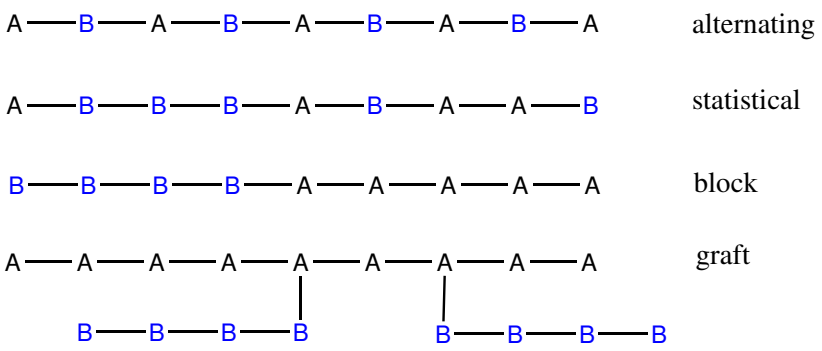

Figure 1.1: Different types of copolymers based on pattern of the chain [2].

One such interesting class of polymers are block copolymers where the repeating units of each respective monomer are arranged into segments of certain length and altering after each other as depicted in picture 1.1

1.1 Self-Assembly of copolymers

The structure of copolymer chain implies, that the conformation of such polymer will depend on properties of the solvent and conditions it is in [3]. Therefore we expect the chain to assemble in order to minimize the free energy of the system. Such logical arrangement of chains as a response to external factors is called self-assembly.
In the case of solvated copolymer we mostly refer to static self-assembly [4], in which the polymer assembles itself and reaches equilibrium at which the final arrangement of chains is stable. Important distinction to make however is that throughout this process there is no energy added to the system and this process happens only due to the effort of minimizing the overall free energy.
In order to achieve the structure that is lowest in energy, the system must balance out all of the forces and interactions that are between two polymer chains or parts of the chain interacting with itself.

1.2 Responsive copolymer systems

Self-assembly of copolymers arranges polymer chains into a stable structure in equilibrium. If we modify the external conditions by changing the concentration, pH, temperature, composition of the mixture et cetera, we might find that in equilibrium, the polymer chains in the system are no longer in the same conformation, but have rearranged as a response to this change. Note that the change of conformation is reversible and if we were to reverse the change, the polymer would go back to it's original arrangement. Copolymers that react to external stimuli in this manner are referred to as responsive systems. This characteristics is mainly caused by different properties of the monomers and also depends on the copolymer pattern. Many of these systems have amphiphilic properties which directly correlate to their responsivness to pH and temperature.
As stated before, these equilibria depend on external conditions of the system, therefore the behaviour of copolymer systems might have unpredictable properties. It is therefore important to study these changes in controlled environments as to separate the respective effects, based on stimuli that caused them.

1.3 pH responsive systems

Due to the amphiphilic nature of copolymer systems with ionizable monomers, we often observe response to change in environment pH.
Given the standard equation for acid-base equilibrium

$$\mathrm{HA} \rightleftharpoons \mathrm{H^+} + \mathrm{A^-}\,,$$

we expect equilibrium shifting in relation to the overall acidity or basicity of the system. We can approach the ionizable segments of copolymer the same way. If the systems contains carboxylic group, we can rewrite the chemical equation as

$$\mathrm{R{-}COOH} \rightleftharpoons \mathrm{R{-}COO^-} + \mathrm{H^+},$$

where R denotes the rest of the polymer chain. At neutral conditions, we assume that carboxylic group will dissociate and reach some degree of dissociation, based on the strength of the acid group. It is very important to note, that behaviour of low-molecular acids and the way they dissociate is not comparable to macromolecular acids [5]. While for low-molecular acids we can safely approximate the degree of dissociation from dissociation constant, $p\mathrm{K_a}$, for macromolecular systems the overall dissociation will be highly dependent on the state of surrounding ionizable chains and their conformation. This phenomena will also be influenced by the temperature responsivity of the copolymer, due to the change of conformation, as will be further discussed.
These changes in dissociation of the ionizable chains will play into the effort of the system to lower it's overall energy and such impact the self-assembly of the copolymer in various ways. Due to these unique properties copolymer systems often display vast amount of responses to the change of pH. We refer to these systems as pH responsive and their variability of ionization is widely used in gelation of pH-dependent diblock copolymer systems [6], tissue engineering [7], pH activated drug release [8] and much more.

1.4 Temperature responsive systems

While the afformentioned changes in ionization contribute greatly to the character of self-assembly process, the behaviour of polymer in solvent is dependent on several other factors as well. First and foremost is the solvent quality in which the polymer is solvated. For the purpose of this work we will distinguish between good solvent, poor solvent and theoretical θ-solvent.
In the conditions of the good solvent, the behaviour of the polymer chain is mostly dictated by interactions between solvent and chain itself (polymer-solvent interaction), whereas in the poor solvent the behaviour is given by interaction of the polymer chains with themselves (polymer-polymer interaction). Theoretical θ-solvent is a hypothetical solvent in which the polymer-solvent and polymer-polymer interactions contribute to the overall behaviour of the system equally [9], [10] .
Solvent quality is often strongly influenced by temperature. This depends mainly on the combination of solvent and polymer system. In these systems we observe phase transition based on temperature. This temperature can be either described as lower critical solution (LCST) temperature or upper critical solution temperature (UCST). LCST refers to a critical temperature below which the polymer is fully soluble in given solvent while UCST refers to a critical temperature beyond which the polymer is fully soluble in given solvent. This phenomena is described by Flory-Huggins solution theory which in addition to describing change in free energy in terms of entropy of mixing also takes into account difference between molecular sizes of solvent and polymer and their respective interactions with each other[11]. It also defines Flory interaction parameter which can be a useful tool for predicting the behaviour of polymer solutions [9].

1.5 Morphology of block copolymers aggregates

One of the most heavily studied copolymer systems are block copolymers mostly due to their segmented nature which can be exploited for multitude of purposes. Amphiphilic block polymers arguably show the most promise. This is mostly due to the the nature of attractions and repulsions between hydrophobic and hydrophilic segments of the polymer chains interacting with each other.
Micelle formation is an important property that is commonly observed in behaviour of block copolymers. Morphology of micelles can range from singular spherical micelles through cylindrical micelles to interconnected micelle networks. The main driving force behind micelle formation in polar solvent is the attraction between hydrophobic segments of the copolymer chains which tend to closely pack themselves into a dense hydrophobic core, which is surrounded by hydrophilic corona. Likewise in nonpolar solvent we can expect hydrophilic core and hydrophobic corona. The overall free energy is minimized and system reaches stable conformation in which interactions of hydrophilic and hydrophobic parts are minimized. This phenomena happens in dilute solutions of block copolymers above concentration that is refered to as critical micelle concentration (cmc) and fixed temperature refered to as critical micelle temperature (cmt). In higher concentrations micelles can further aggregate into gels and corresponding concentration is refered to as critical gel concentration (cgc).

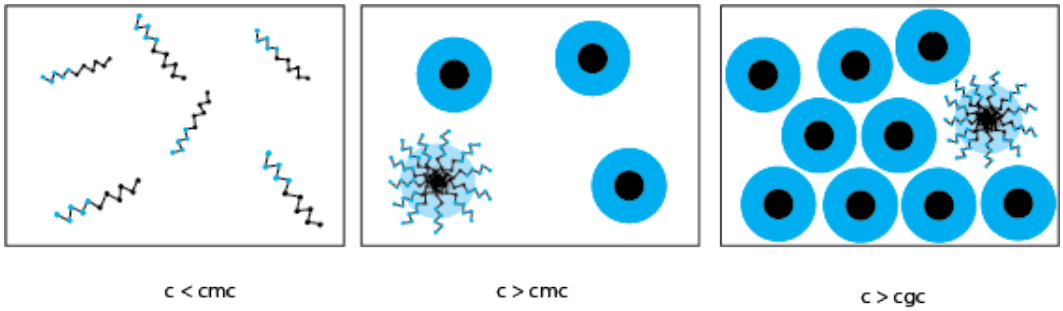

Figure 1.2: Micelle formation at different concentrations. Left picture depicts lone polymer chains in solvent, middle picture depicts formation of micelles above the critical micelle concentration while picture on the right depicts micelles above critical gel concentration.

Micelle formation is often affected by the systems responsivity to different stimuli. Thermo-responsive systems in which micelles are formed can undergo several different conformational changes based on temperature ranging from interlinking or formation of cylindrical micelles to complete breakdown of the micelles. These changes of conformation are studied because of the ability to solvate or coat otherwise insoluble particles. They are also exploited as potential drug-carries due to their possible thermal breakdown resulting in release of the drug. *p*H responsive systems can offer structural changes based on electrostatic interactions caused by hydrophilic segments. For example micelles with acidic groups can often undergo swelling as a result of high hydration of carboxylic groups. These properties are exploited a potential desalination agents.

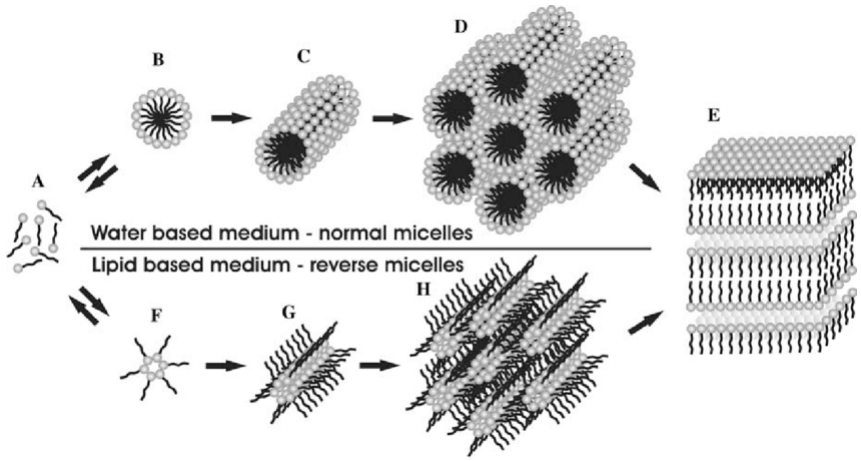

Figure 1.3: Possible micelle structures based on medium in which polymer is solvated.[12]

1.6 Cryo electron microscopy

Gaining insights into the structural properties of soft matter systems has posed significant challenges. While methods like dynamic light scattering provide valuable information regarding the particle size and shape, cryo electron microscopy has emerged as a central imaging technique in recent years. This method enables the direct imaging of aggregate-specific details in soft matter systems, which often contain water and pose difficulties for conventional electron microscopy, mainly due to the presence of vacuum in the microscope chamber. In many cases, the crucial information would be gained only in case of the analysis of the sample at the same conditions as in solution, which is possible after rapid freezing of it in cryo conditions [13], [14].
In classic electron microscopy, the imaged specimen must endure the vacuum chamber's low pressure and the energy transmitted by the electron beam. As mentioned beofre, this frequently results in sample deformation and inaccurate images. Cryo electron microscopy addresses this issue by rapidly freezing the sample using liquid nitrogen, creating a thin layer of vitreous ice. This quick freezing process effectively immobilizes the structures in place without changing of their size and shape compared to the real-life conditions. The benefits of this method were recognized by recieving Nobel prize in biology in 2017.[15] The application of cryo electron microscopy is particularly advantageous for studying the self-assembly of soft matter systems. It allows researchers to observe the structures frozen, and thus stabilized under various conditions that may exist within the sample. By examining different sets of conditions, such as pH, temperature, concentrations, etc., a more comprehensive understanding of these systems can be achieved. Cryo electron microscopy is a powerful method for studying soft matter systems, however it necessitates meticulous sample preparation under controlled conditions [16].

The success of cryo electron microscopy relies on precise sample handling and preparation. The specimen needs to be carefully prepared in a way that preserves its native structure and composition. This involves subjecting the sample to rapid freezing in a controlled environment to form thin, transparent to electrons layer of vitreous ice. This process is called cryo plunging. The freezing process must be fast enough to prevent the formation of ice crystals, which could distort the delicate structures of the soft matter system.The controlled conditions during sample preparation are crucial to ensure the accuracy and reliability of the resulting images. Any variations or inconsistencies in the freezing process or sample handling can lead to artifacts or distortions that may compromise the interpretation of the data [17].

Therefore, researchers employing cryo electron microscopy must exercise great care in every step of the sample preparation process, from sample selection to vitrification, to obtain high-quality images that reliably represent the structural properties of the soft matter system under investigation.

2. Methods

Our research focused on the study of self-assembly and properties of a block copolymer known as Poly(acrylic acid-block-N-isopropylacrylamide) (PAA-PNIPAm). We aimed to understand how this copolymer undergoes self-assembly under varying polymer concentrations and meso-tetrakis(N-methyl-4-pyridyl)porphine tetrakis(p-toluenesulfonate) salt content. To achieve this, we conducted experimental work using electron microscopy. Specifically, we compared samples of PAA-PNIPAm in sodium hydroxide solution at different temperatures. Additionally, we employed computer simulations for theoretical analysis, exploring the effects of different stimuli on the system. In the following chapter, we will provide a detailed description of the methods used throughout our study.

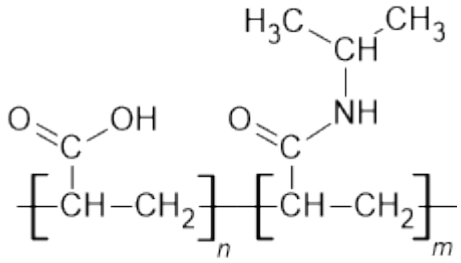

Figure 2.1: Structure of block copolymer PAA-PNIPAm

2.1 Experimental

2.1.1 Scanning Transmission Electron Microscopy

Scanning Transmission Electron Microscopy (STEM) involves scanning a focused electron beam through a thin sample specimen in a raster pattern. During this process, the beam interacts with the sample, and the transmitted electrons carry valuable information about this interaction [18]. The transmitted electrons are collected by a detector positioned below the sample, where they generate a signal used to form an image. By detecting and recording these transmitted electrons, STEM enables the creation of detailed images that reveal the structure and properties of the sample. STEM also allows for acquisition of multiple types of signals as secondary electrons, backscattered electrons, and characteristic X-rays emitted by the specimen [19].

2.1.2 Scanning Transmission Electron Microscopy in cryo conditions

STEM, while a powerful imaging technique for many systems, presents challenges when imaging a PAA-PNIPAm solution. STEM utilizes a focused beam of high-energy electrons that scans the sample in a raster pattern. However, this high-energy beam is likely to cause destruction or alteration of the composition of our

system. Since our system is a solution and our main objective is to study its behavior in solution, conventional STEM imaging is unsuitable for our purposes.

To address this issue, we will employ cryogenic conditions in conjunction with STEM. This method involves rapidly freezing the sample in liquid nitrogen, effectively preserving the structures in their current conformations and encasing the specimen in a thin layer of vitreous ice. Subsequently, we will conduct STEM imaging on this cryo-preserved sample while maintaining a low temperature (approximately -173 °C) within the sample chamber. By doing so, we can obtain the most accurate representation of our sample without compromising its integrity.

The sample preparation method involves usage of a mist chamber to prepare the sample in moist environment. A small amount of PAA-PNIPAm solution is applied onto a carbon mesh within the chamber. The mesh, along with the sample, is then automatically blotted against a filter paper to ensure that the prepared specimen is thin enough for imaging. Subsequently, the sample is left undisturbed for approximately two minutes to allow for relaxation [17].

After the relaxation period, the sample is vitrified by plunge freezing it in liquid ethane. The vitrified specimen is loaded into a cryo holder, which was previously regenerated to ensure good isolation properties and filled with liquid nitrogen. Throughout the imaging process the prepared sample is maintained at a temperature of -173 °C.

For our experimental set-up scanning transmission electron microscopy images were acquired using a JEOL NEOARM 200 F microscope equipped with a Schottky-type field emission gun at an accelerating voltage of 200 kV. Samples were prepared by rapid freezing using a Leica EM GP2 cryo plunger. Carbon coated copper grids were loaded into the specimen chamber under humid conditions to avoid sample drying. Grids were glow-discharged using a Leica EM ACE600 vacuum sputter coater prior to sample loading. A drop of sample solution was placed on the grid, blotted 10 times by automatic blotting arm, and then rapidly plunged into the liquid ethane kept at the temperature of liquid nitrogen. Sample was transferred to Fischione Cryo Transfer Tomography Holder Model 2550 and then inserted into the electron microscope. The cryo holder dewar was refilled with liquid nitrogen during the whole time of the sample imaging to ensure the optimum cooling conditions.

2.2 Computer simulations

2.2.1 Coarse modelling of polymer system

Simulating complex macromolecular systems at the atomic scale is computationally demanding, primarily due to the intricate nature of large polymer chains. The properties observed in these macromolecular chains are a direct consequence of their atomic composition. The ideal approach to simulate such systems would be to recreate the chain as reliably as possible down to the atomic level, computing the interactions between all atoms to determine the overall energy. However, several challenges hinder this approach. The primary obstacle is the absence of a suitable model that can effectively account for the attractive and repulsive forces between all atoms in the system while still being computationally feasible. The sheer scale of macromolecular simulations makes it impractical to implement such

a detailed model. Consequently, we employ a series of approximations to reduce computational time while maintaining a reasonable level of detail [20]. The specific approximations employed depend on the purpose of the simulations.
One such method is coarse grained modeling [21]. The fundamental concept behind this approach is to simplify the complexity of the system by reducing the level of detail in the representation, while still ensuring that the essential characteristics and behavior of the segment are accurately captured [22]. In the context of copolymer chains, this approach involves approximating segments that share similar properties by using simpler representations while preserving the essential characteristics of the segment. We approximate the repeating units of the same type within the copolymer chain as soft spheres, ensuring that their dissociative, electrostatic, and other defining properties (or suitable approximations) remain intact. The overall model for computing repulsive and attractive forces along with dissociation of ionizable segments will be discussed in following sections.

2.2.2 Monte Carlo

Basics

The Monte Carlo method is a computational technique employed for solving problems characterized by inherent non-determinism. It leverages random number generation to sample values within specified ranges for variables of interest. Through iterative cycles, these randomly generated values are used to perform deterministic calculations, allowing for the evaluation of observable phenomena [23]. In the most basic Monte Carlo algorithm we can describe the process of computing as follows. The first step involves identifying the variables that are relevant to the problem at hand and determining their specific ranges or possible values. Once these variables and their ranges are defined, the next step is to generate random values for each variable. Generated values are then used in deterministic calculations. This is done over many iterative cycles, while collecting large amount of data which is then used to determine average values of properties depending on studied matter at hand [24]. One simple example would be computing roll of two dice by generating two random numbers in range from 1 to 6 and then saving the overall sum. For each of the possible outcomes (2-12) a counter would increase by one whenever this outcome occurs. We would then compute this behaviour over many iterative cycles. After certain amount of dice rolls (cycles) we would see that the results begin to resemble probability distribution of all of the possible outcomes. We see that even with random number generation we can observe some of the inherent behaviours of the system.

Importance sampling

The aforementioned algorithm for generating random values within an acceptable range for variables, or also sometimes referred to as brute force Monte Carlo, is however flawed for simulating large systems of molecular interactions. Let us consider an example system of n atoms. We can safely assume that the overall energy of such system will be a function of coordinates of all of the atoms $U(r_i)$, where r_i denotes the vector of coordinates for corresponding atoms $r_i = (x_i, y_i, z_i)$.

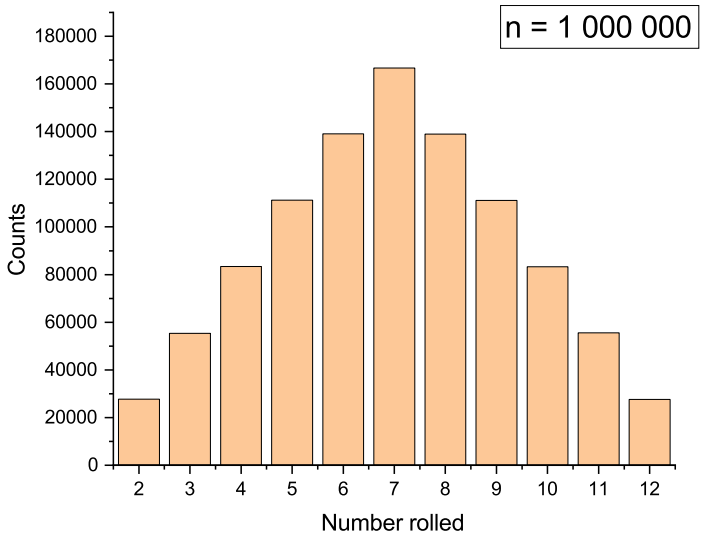

Figure 2.2: Proposed roll of two dice over 1 million iterative cycles. Columns represent counts of each outcome. Probabilities would be simply calculated by dividing the number of occurences by number of cycles.

If we take into account only repulsive and attractive forces between atoms that are dependent solely on distance, we can write equation for overall energy as

$$U = \sum_{i=0}^{i=n} \sum_{j=i+1}^{j=n} U(r_i, r_j),\ i \neq j, \tag{2.1}$$

where we sum the overall energy over all possible pairings of atoms. Now we will generate random values by which we will change the coordinates of the atoms and therefore move the particles around. Even in this simple example we can find a fatal flaw. This algorithm doesn't in any way differentiate between configurations that are energetically favourable and configurations that are energetically unfavourable. In this particular system, there is no concept of equilibrium as the probabilities of the system being in any specific state are equal across all states [25]. To fix this, we deploy Metropolis Method [26].

Metropolis method

In the Metropolis method, we take into account the probability distribution of the potential states that our system can occupy. As a result, during the simulation, we include a step where we make a decision regarding whether to accept a proposed transition. If we continued in the simple example of atoms mentioned previously. We can calculate the overall change in system energy that resulted from movement of the atoms. If this change of energy is negative, we would simply accept such configuration. If however the energy of the proposed configuration was higher, we can use Boltzmann factor defined as

$$\frac{p_i}{p_j} = \exp^{\frac{\Delta E}{k_b T}}, \tag{2.2}$$

and accept the proposed change with this probability.

2.2.3 Molecular Dynamics

An alternative strategy for simulating molecular systems involves treating them as classical many-body systems. This approach becomes feasible for sufficiently large systems, where concerns regarding rotational and vibrational motions, which would introduce quantum effects and compromise the accuracy of our results, can be disregarded. This methodology is known as molecular dynamics. By adopting a classical framework, we utilize Newton's laws of motion to describe the behavior of the simulated molecular systems. Through numerical integration, we calculate the relevant data necessary for addressing the specific problem at hand. This method can be simplified into 4 steps. First, we generate the initial positions and velocities of the bodies, such as atoms or other representations. While random generation can be used, it is preferable to implement a mechanism that ensures the generated particles are not in very close proximity to each other or overlapping.

Next, we compute the forces acting on the bodies. There are various versions of force field approximations that can be employed for this purpose. These models compute the potential energy of two atoms (or other representations) based on distance between them. As an example, we can consider force field model based on the Lennard-Jones potential [24] (see figure 2.3) Force fields typically involve the introduction of a cutoff distance. This distance is used to limit the calculation of the potential beyond a certain point, thus avoiding unnecessary computations that do not significantly contribute to the overall force.

By following these steps, we can simulate the behavior and interactions of the particles within the system..

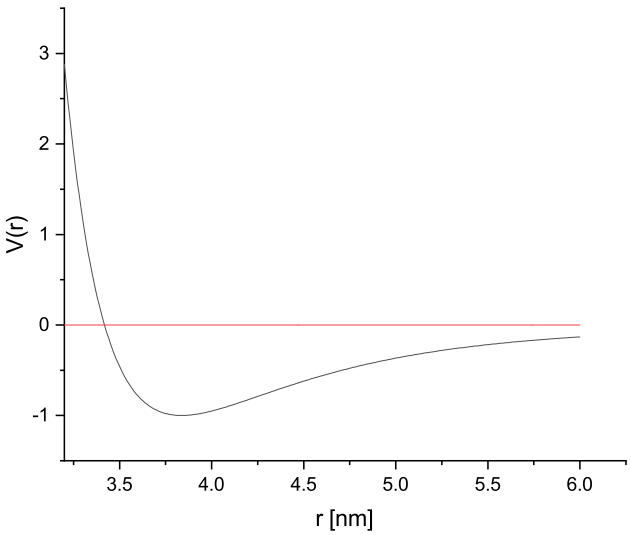

Figure 2.3: Lennard-Jones potential model for non-bonding force of neutral atoms. $V(r)$ denotes potential energy and r denotes separation of two atoms.

Once the forces affecting the bodies are computed, we can proceed to integrate Newton's second law of motion and predict the positions of the particles at a new time. One commonly used integration method is the Verlet method [25], which

can be expressed mathematically as follows:

$$\vec{r_i}(t+h) = 2\vec{r_i}(t) - \vec{r_i}(t-h) + h^2 \frac{\vec{f_i}(t)}{m_i}, \tag{2.3}$$

where $\vec{r_i}(t)$ denotes position of particle i at a time t, h denotes one time step and $\vec{f_i}$, m_i denote forces affecting the particle and mass of the particle respectively. The process is repeated until equilibrium is attained, and at that point, we can extract data that offers valuable insights into the system's properties.

2.2.4 Hamiltonian Monte Carlo

The Monte Carlo method, while valuable for generating insights into complex systems, relies on random walk behavior for proposing configuration changes. However, this random walk behavior can be improved by sampling from a probability distribution and evaluating the acceptance probability of configuration changes. Despite these enhancements, Monte Carlo simulations can still be computationally demanding and may only explore the system to a limited extent. In contrast, Hamiltonian Monte Carlo offers a more efficient approach for proposing configuration changes, leading to enhanced exploration of the system and improved computational performance. The fundamental distinction between the Monte Carlo method and Hamiltonian Monte Carlo lies in the generation of proposals for the Metropolis criterion. While the classic Monte Carlo method employs random number generators for generating proposals, Hamiltonian Monte Carlo generates proposals by implementing molecular dynamics time evolution. This time evolution is calculated through the same process discussed earlier in the section on molecular dynamics, involving a specified number of steps using a chosen integrator. This integration procedure incorporates the system's dynamics, including positions and velocities, to produce meaningful proposals for configuration changes. This utilization of molecular dynamics-based proposals enables Hamiltonian Monte Carlo to explore the system more effectively and generate samples that better represent the target distribution compared to traditional Monte Carlo methods relying solely on random number generators [27].

2.2.5 Reaction Monte Carlo

To simulate the dissociation reaction $\mathrm{R{-}COOH} \rightleftharpoons \mathrm{R{-}COO^- + H^+}$ in a Monte Carlo simulation, the traditional canonical ensemble Monte Carlo method faces a challenge due to the fixed number of molecules in the system. To overcome this problem efficiently, the reaction ensemble Monte Carlo method can be employed. This method involves modifying the Monte Carlo algorithm to incorporate reaction moves alongside translational moves [28].

The reaction ensemble Monte Carlo method starts by randomly selecting whether the next move will be a translational move or a reaction move. If a translational move is chosen, the basic Monte Carlo algorithm proceeds by proposing a new configuration based on the movement of molecules within the system.

On the other hand, if a reaction move is chosen, the algorithm randomly determines whether it will be a forward reaction move or a backward reaction move. In a forward reaction move, a randomly selected non-ionized monomer

becomes ionized, and an H^+ ion is inserted into the simulation box at a random position. In a backward reaction move, a randomly selected H^+ ion is removed, and a randomly selected monomer is de-ionized.

The acceptance of a reaction move is determined by a probability criterion

$$P^{\xi} = \min\left(1, V^{\overline{\nu}\xi}\Gamma^{\xi}\exp\left(-\beta\Delta U\right)\prod_{i=1}\frac{N_i^0!}{(N_i^0+\nu_i\xi)!}\right), \tag{2.4}$$

where ΔU is the change of interaction energy, $\beta = \frac{1}{k_bT}$, ν_i is negative (for reactants) or positive (for products) stoichiometric coefficient of species i, $\overline{\nu} = \sum \nu_i$, V is simulation box volume. Extent of reaction ξ connects intial number of species i to the current number N_i as

$$N_i = N_i^0 + \nu_i\xi \tag{2.5}$$

Γ can be written out as

$$\Gamma = K_A\Big(\frac{p}{N_A k_b T}\Big)^{\overline{\nu}}, \tag{2.6}$$

where N_A is Avogadro number and p is pressure [29].

2.2.6 Proposed model for computer simulations

Polymer model

In our polymer approximation, we employ a coarse-grained model, wherein individual monomers are represented as soft spheres. These monomers interact through various forces, including Coulombic interactions, bonding interactions, and non-bonding interactions. It's worth noting that the particles belonging to the PAA and PNIPAm blocks exhibit distinct non-bonding interactions and reaction capabilities. The solvent in our simulation is considered to be structureless, and its properties are determined by its relative permittivity. All particles are contained within a simulation box, which adheres to periodic boundary conditions, ensuring a continuous and consistent environment for the system.
Bonding potential for the beads is harmonic potential

$$U_b = \epsilon_b(r - r_0)^2, \tag{2.7}$$

where $\epsilon_b = 80.0\,k_BT$ is the strength of massless spring, r denotes the instantenous distance between two beads and $r_0 = 0.3$ nm is the distance at which the potential energy U_b is at minimum. We compute non-bonding potential energy U_nb as

$$U_{nb} = \epsilon_{nb}\frac{(r - r_c)^2}{r^2}\,, r < r_c, \tag{2.8}$$

where $\epsilon_{nb} = 1.0\,k_BT$, r is the distance between two beads and $r_c = 2r_0$ is cut-off distance beyond which $U_{nb} = 0$.
To simulate different solvent conditions we modify hydrophobicity of PNIPAm beads as follows :

$$U_{nb} = U(attr.) + U(rep.), \tag{2.9}$$

where $U(rep.)$ is standard repulsive potential calculated in eqn. 2.8 and $U(attr.)$ is calculated as

$$U(attr.) = \epsilon_{nb}\tau_p\frac{(r - 2r_c)^2}{r^2}\,, r < r_c, \tag{2.10}$$

where τ_p is the parameter scaling the properties of the solvent, where athermal solvent corresponds to $\tau_p = 0$ and theta solvent is approximately $\tau_p = 0.068$ [30]. Overall electrostatic interactions were evaluated by Ewald summation [31].

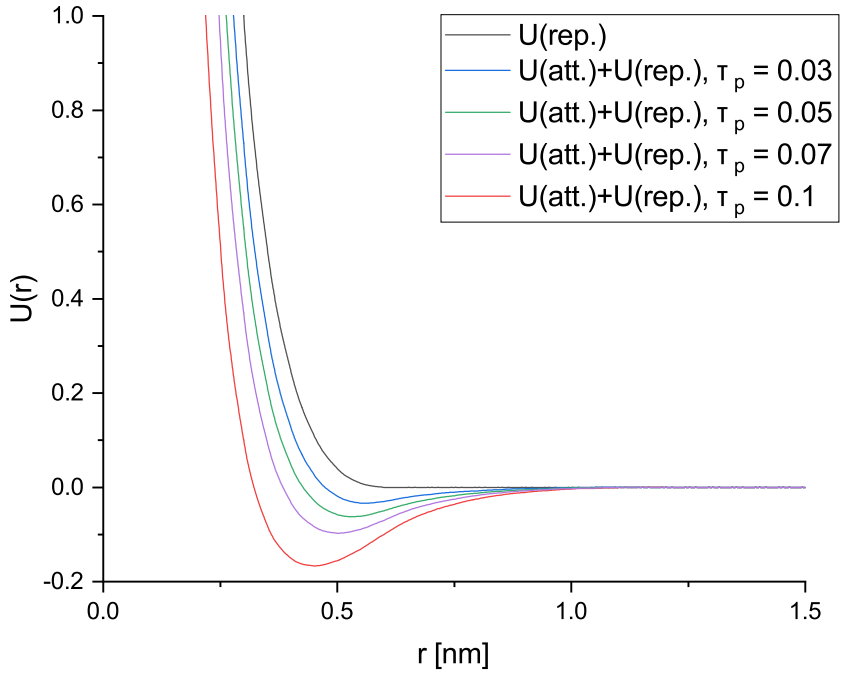

Figure 2.4: Potentials dependent on distance of the two beads r for different τ_p parameters and pure repulsive potential also dependent on distance r.

To represent the ratio of the PAA beads and PNIPAm beads we used experimental findings which can be found in figure 2.5. In this study, we made certain assumptions based on these findings. First we calculated the ratio of PAA/PNIPAm segments based on polymer used in these results. We assumed the ratio of poly(acrylic acid) (PAA) to poly(N-isopropylacrylamide) (PNIPAm) in the copolymer to be 0.4/0.6. The copolymer chain length was fixed at 60 beads, which translates to 24 beads of PAA and 36 beads of PNIPAm. We then investigated the behavior by varying the parameter τ_p in the range from 0.01 to 0.1. Our aim was to understand the effects of temperature on the copolymer, and we approximated the temperature change by increasing hydrophobic properties of the PNIPAm segments present in the PAA-PNIPAm copolymer. By changing τ_p parameter we increased the attraction of hydrophobic chains which we used as an approximation of behaviour of PNIPAm blocks in the real polymer with rising temperatures. For the PAA segments of the polymer chain we use $pK_\mathrm{A} = 4.5$ [33], which was recalculated according to the section 2.2.5. To mimic basic conditions $p\mathrm{H} = 9$ we calculate Γ parameter with $pK_\mathrm{A} = 2.5$ to maintain the difference in $p\mathrm{H}$

We conducted a study on two different architectures. Initially, we examined linear copolymer chains with varying concentrations and salt levels. Subsequently, we approximated the structure of micelles by creating a star architecture, wherein

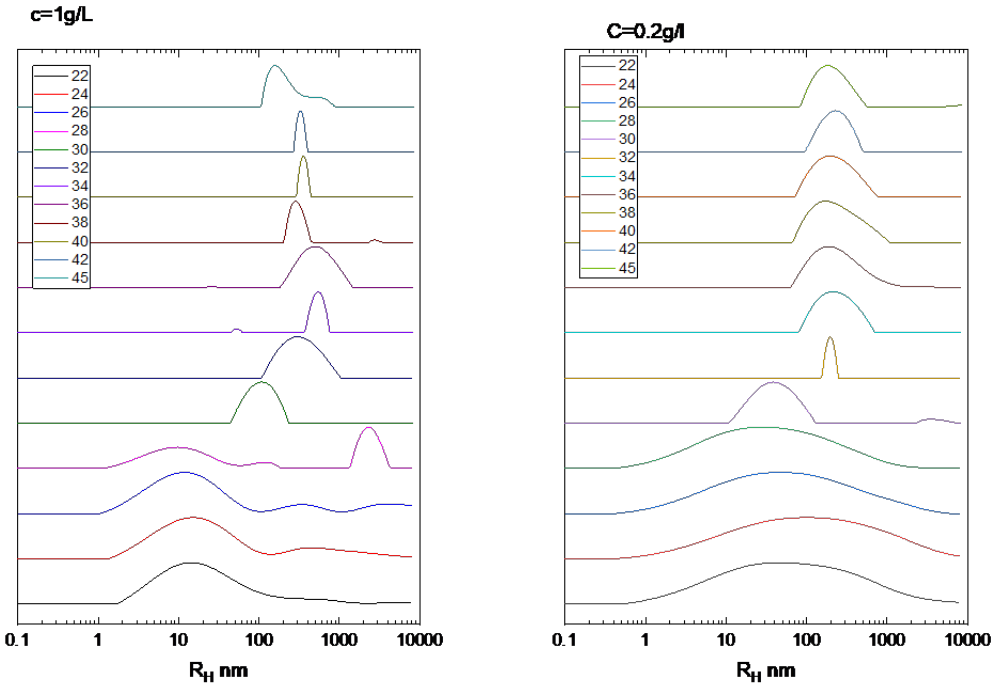

(a) (b)

Figure 2.5: DLS measurements of hydrodynamic radius of PAA-PNIPAm solution with meso-tetrakis(N-methyl-4-pyridyl)porphine tetrakis(p-toluenesulfonate) (TMPyP) salt content of $7.41 \cdot 10^{-6}$ (a) concentration of polymer 1.0 g/l (b) concentration of polymer 0.2 g/l °C [32]

the PNIPAm blocks were connected to a central bead serving as the origin point. Each star architecture comprised 10 copolymer chains, with each chain consisting of 60 beads.

2.2.7 Simulation protocol

We conducted all of simulations by using Hamiltonian Monte Carlo in reaction ensemble. We used Hamiltonian Monte carlo implementation by Soft Matter Theory research group from Charles University in Prague [34]. The algorithm for these simulations is as follows. Initially, a choice is made with equal probability between a conformational step or a reaction step. In the conformational step, a proposal for the Metropolis criterion is generated by performing multiple molecular dynamic steps. In our case, we have selected 100 steps for one Monte Carlo proposal, where each step is 0.05 time simulation units. This proposal is then evaluated using the Metropolis criterion, and acceptance or rejection is determined based on the probability derived from Boltzmann's probability distribution. In the reaction step, a direction for the reaction is randomly chosen with equal probability. Depending on the selected direction, one of two actions is taken. If the chosen direction is to ionize, a random non-ionized PAA bead is selected, and an H^+ bead is inserted at a random location within the simulation box. If the chosen direction is to de-ionize, a random ionized PAA bead is selected, and the corresponding H^+ bead is removed. These actions are performed based on the specified direction and the type of bead (ionized or non-ionized) selected randomly. Then the proposal is passed to the Metropolis criterion and evaluated in the same way as conformational step.

2.2.8 Data collection and evaluation

In simulations such as Hamiltonian Monte Carlo, data collection and evaluation require careful consideration due to the presence of correlation in the generated data. The commonly used method of calculating standard deviation, σ_X, given by

$$\sigma_X^2 = \langle (\overline{X} - \langle X \rangle)^2 \rangle, \tag{2.11}$$

is not applicable in this case. To address this issue, we employ the block method for estimating the standard deviation. This approach involves dividing the data into blocks based on their correlation time, which represents the number of steps at which the data exhibits significant changes. More precisely, the correlation time can be mathematically defined as

$$\tau = \sum_{k=1}^{\infty} c_k, \tag{2.12}$$

where

$$c_k = \frac{\langle \Delta X_i \Delta X_{i+k} \rangle}{\langle \Delta X^2 \rangle}. \tag{2.13}$$

Here, ΔX_i denotes the deviation of a data point X_i from its mean, and can be approximated as $\Delta X_i \simeq X_i - \overline{X}$, and c_k represents the correlation coefficient between two data points separated by k steps [35]. Statistical calculations are then done on these blocks. By employing the block method and considering the correlation time, we can effectively handle the correlation in the data and accurately estimate the standard deviation.It is crucial to emphasize that data collection was specifically focused on states where the system reached equilibrium. This deliberate selection aims to minimize potential errors during data processing.

By exclusively considering equilibrium states, we enhance the reliability of the collected data and ensure its suitability for subsequent analysis and calculations. Small preview of the sampling data of radius of gyration time evolution, where we investigate the validity of the data, can be found in attachment 4.1 .

3. Results and discussion

In the subsequent chapter, we aim to present our findings from both computer simulations and electron microscopy imaging. In the computer simulations section, we will provide measured values along with their variability under various conditions. Specifically, we investigate changes influenced by concentration and salt content as stimuli and changes influenced by initial architecture as approximation of linear chains and micelles. Additionally, we briefly discuss the qualitative results regarding the influence of solution pH, although it was not the primary focus of our study. In the end we qualitatively verify the predictions made by star architecture by simulating clusters of PAA-PNIPAm chains.

In the electron microscopy section, we compare images captured at temperatures of 25 °C and 50 °C in a sodium hydroxide solution. Furthermore, we compare the size distributions of particles observed at these two temperatures.

3.1 Concentration dependence

We conducted investigations on two simulation sets, where the primary difference was the concentration of the solution. One set was carried out at a concentration of 1.0 g/l, and the other at 0.1 g/l. Within each concentration, we examined two possible architectures: linear chain and star. Both sets contained poly(acrylic acid) segments; we further split the simulations into two more sets, with differing pK_{A} values of 4.5 for the first set, and 2.5 for the second set. The first set approximates the standard pK_{A} of poly(acrylic acid) in a polymer chain, while the second set approximates a highly ionized polymer chain under basic conditions. These simulations were carried out with different initial architectures to investigate the behaviour of linear chains and micelles (approximated as star architecture). We simulate over range of τ_p parameter from 0.01 to 0.1 as an approximation of temperature, where we associate rise in τ_p with rise in temperature.

3.1.1 Change of radius of gyration induced by change in concentration

Linear chain architecture

In the case of linear chains, we observed similar behavior for both concentrations, 0.1 g/l and 1.0 g/l. As expected, we noticed a decrease in the square of radius of gyration ($\mathrm{R}_{\mathrm{g}}^2$) as the τ_p parameter increased. Measured data can be viewed in figure 3.1.
It is worth noting that the data set exhibited a relatively large standard deviation. However, this can be attributed to the fact that at low τ_p, which we associate with low temperature, the chains did not exhibit any specific preferred conformation. This limitation did not hinder our ability to study the mean values of the radius of gyration in which we observed said trends and believe to be accurate representation of the system.

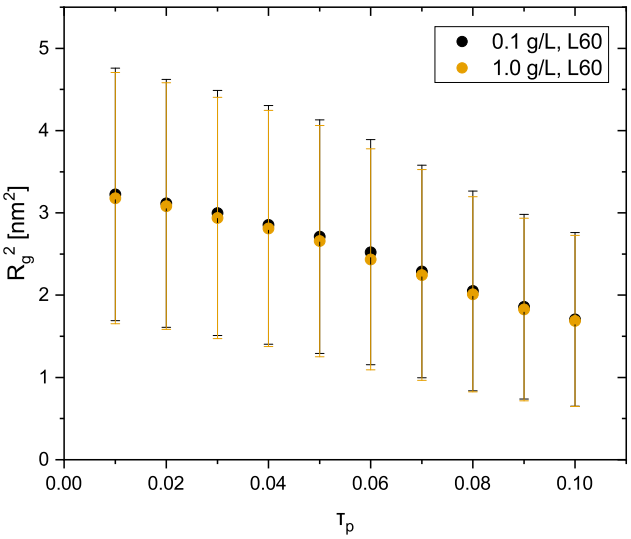

Figure 3.1: R_g^2 in relation to increasing τ_p parameter at $pK_A = 4.5$. L60 denotes linear chains consisting of 60 beads. In yellow is concentration of 1.0 g/l and in black is concentration of 0.1 g/l

As we increased the τ_p values, the system exhibited a preference for conformations characterized by small hydrophobic PNIPAM segments forming cores. To provide visual clarity, we have included snapshots that depict the typical polymer chain conformation at different τ_p values in the system in figure 3.2. For future reference we used gray color for un-ionized bead, blue color for ionized bead, yellow color for salt beads and green color for H^+ beads as representations in snapshots from simulations.

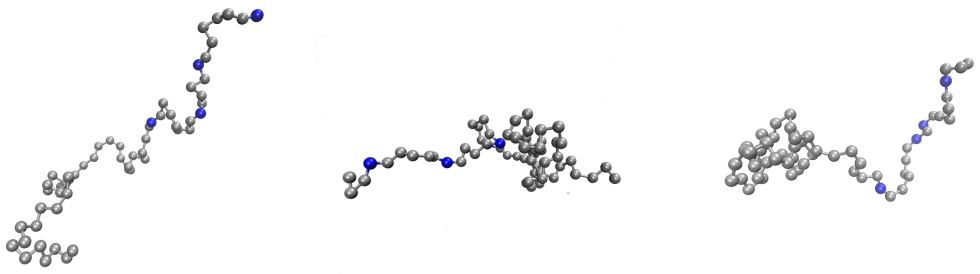

(a) (b) (c)

Figure 3.2: Snapshots of linear chains at different τ_p parameters and $pK_A = 4.5$ (a) $\tau_p = 0.01$ (b) $\tau_p = 0.05$ (c) $\tau_p = 0.1$

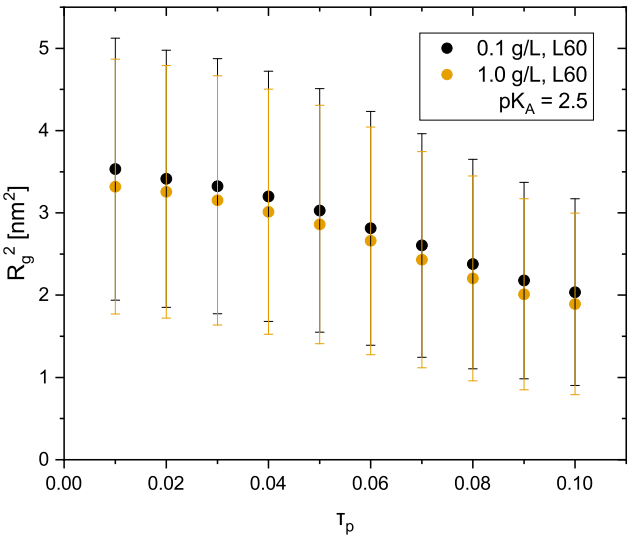

Figure 3.3: R_g^2 in relation to increasing τ_p parameter in basic solution approximated as $pK_A = 2.5$. L60 denotes linear chains consisting of 60 beads. In yellow is concentration of 1.0 g/l and in black is concentration of 0.1 g/l

In the simulations of the system with lower pK_A values, approximating an ionized chain in basic conditions, we observed ever so slight increase in the average value of the R_g^2. This can be primarily attributed to the ionization of the PAA segments, which causes them to stretch out and contribute to the increased size of the polymer chain.

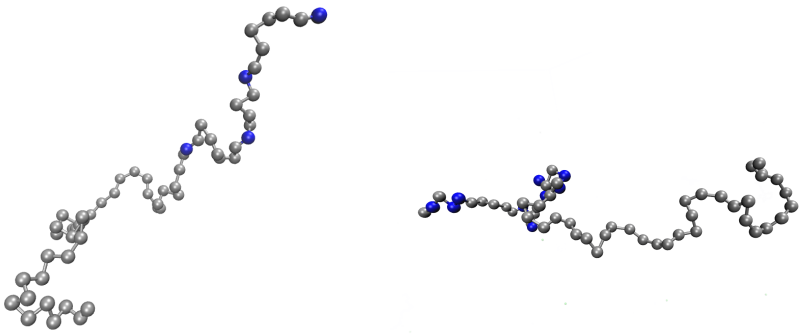

(a) (b)

Figure 3.4: Snapshots of linear chains at different pK_A values at $\tau_p = 0.01$ (a) $pK_A = 4.5$ (b) $pK_A = 2.5$

Star architecture

In the case of the star architecture, we observed similar trends of radius of gyration values for both 0.1 g/l and 1.0 g/l concentrations. Considering the nature of the star architecture, it is expected that the measured values would be larger in magnitude compared to linear chains. The slight increase in the radius of gyration observed in the simulation with a concentration of 0.1 g/l can be attributed to higher ionization within the less concentrated system. As a result, the polymer chains stretch more, leading to an increase in their overall size. We observed a

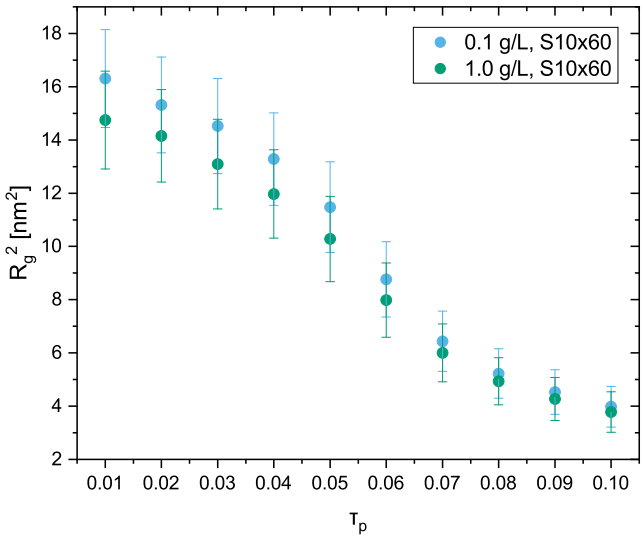

Figure 3.5: R_g^2 in relation to increasing τ_p parameter and $pK_A = 4.5$. S10x60 denotes star architecture consisting of 10 chains with 60 beads each. In green is concentration of 1.0 g/l and in blue is concentration of 0.1 g/l

decrease in R_g^2 as the τ_p parameter increased. This trend resulted in the formation of dense cores, particularly at high τ_p values, which we associate with higher temperatures. We interpret this core formation as indicative of a transition from a solvated state.

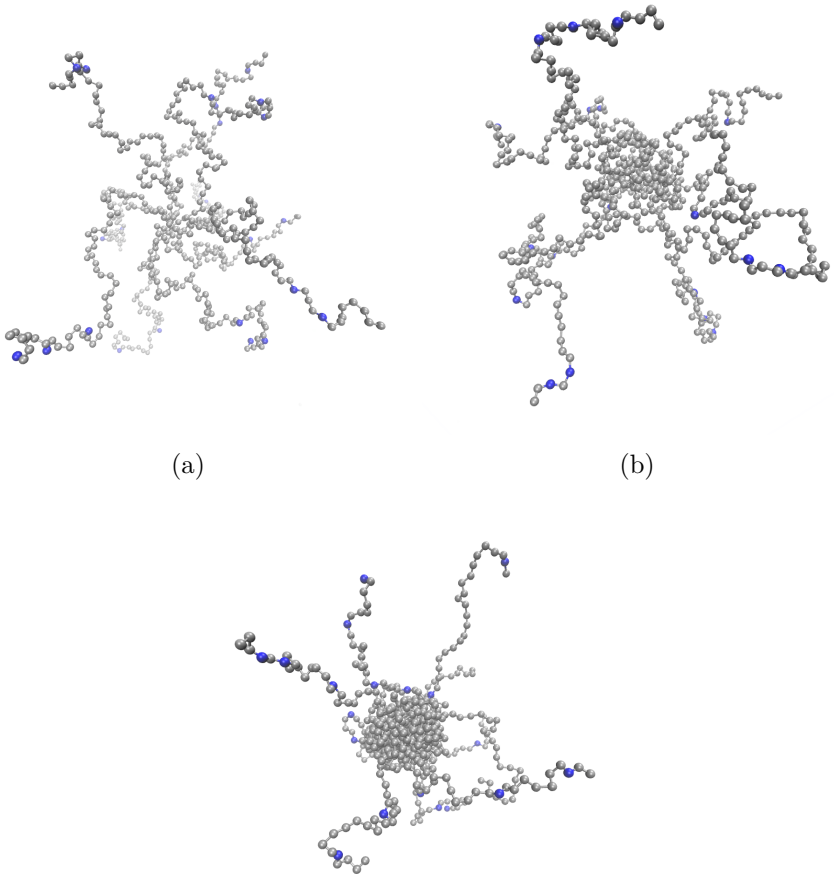

(a) (b)

(c)

Figure 3.6: Snapshots of stars at different τ_p parameters (a) $\tau_p = 0.01$ (b) $\tau_p = 0.05$ (c) $\tau_p = 0.1$

In the simulations with decreased pK_A, we observed a significant increase in the radius of gyration. Additionally, we noticed a greater increase in the radius of gyration for the 0.1 g/l concentration. We attribute this observation to the higher possibility of ionization, which in turn leads to the stretching out of the polymer chains. We demonstrate this in figure 3.8

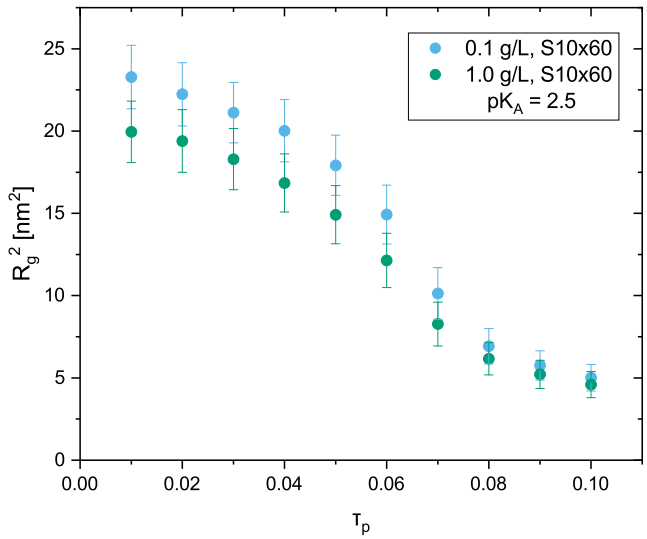

Figure 3.7: R_g^2 in relation to increasing τ_p parameter and $pK_A = 2.5$. S10x60 denotes star architecture consisting of 10 chains with 60 beads each. In green is concentration of 1.0 g/l and in blue is concentration of 0.1 g/l

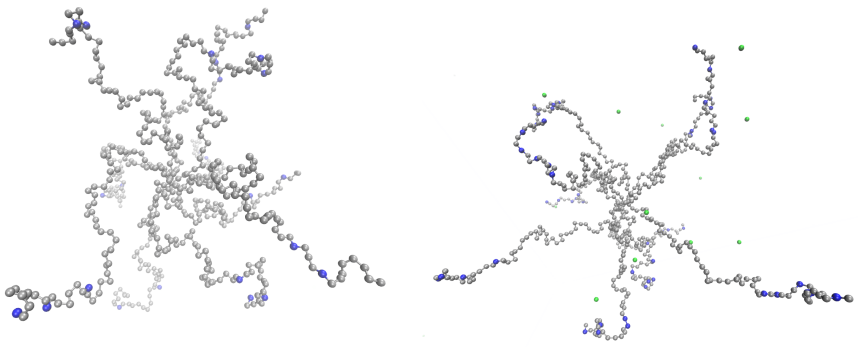

(a) (b)

Figure 3.8: Snapshots of linear chains at different pK_A values at $\tau_p = 0.01$ (a) $pK_A = 4.5$ (b) $pK_A = 2.5$

3.1.2 Change of degree of ionization induced by concentration

We examined the same simulations to analyze the influence of change in concentration on the degree of ionization. The outcomes obtained align with our anticipated expectations. As anticipated, we observed an elevation in the degree

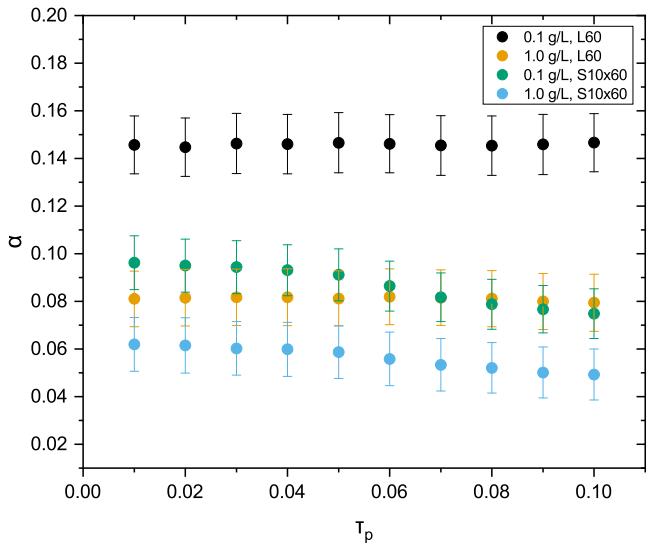

Figure 3.9: Degree of ionization in relation to τ_p parameter at $pK_A = 4.5$. S10x60 denotes star architecture consisting of 10 chains with 60 beads each and L60 denotes linear chains of 60 beads each. Color scheme remains the same as previous plotted data.

of ionization for both linear chains and star architectures as the concentration decreased from 1.0 g/l to 0.1 g/l. However, an interesting finding emerged when examining the star architecture with an increase in the τ_p parameter. In this case, we noticed a slight decrease in the overall degree of ionization. We attribute this phenomenon to the formation of hydrophobic cores, which restrict the movement of the PAA segments. Consequently, the influence of the chains on each other becomes more pronounced, leading to the observed decrease in degree of ionization.

As for simulations with lower pK_{A} value, we again arrive at the same conclusion. With the distinction that affomentioned changes become more pronounced as a direct consequence of higher degree of ionization.

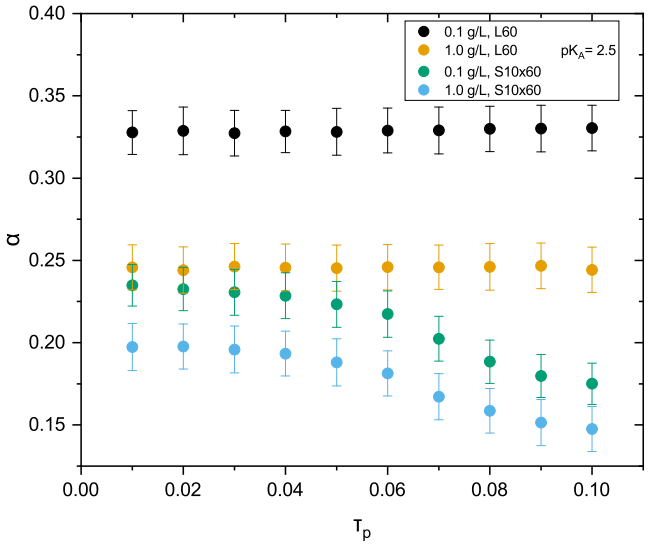

Figure 3.10: Degree of ionization in relation to τ_p parameter at $pK_{\mathrm{A}} = 4.5$. S10x60 denotes star architecture consisting of 10 chains with 60 beads each and L60 denotes linear chains of 60 beads each. Color scheme remains the same as previous plotted data.

3.2 Salt presence dependence

In our continued investigation, we conducted simulations using two different sets of concentrations: 1.0 g/l and 0.1 g/l. The purpose was to examine the effects of introducing salt into the solution. In these simulations, we added 4^+ ions to the system. It's worth noting that there was a difference in salt concentrations between the two sets of simulations. At a concentration of 1.0 g/l, the salt concentration was set to 10^{-4} M. For the 0.1 g/l concentration, the salt concentration was set to 10^{-6} M. This choice was made because simulations at 1.0 g/l concentration proved to be computationally challenging when using a salt concentration that matched the 0.1 g/l set. Additionally, we modified this set of simulations similarly to the concentration-dependent set by adjusting the pK_A to 2.5. This alteration was made to approximate a basic solution. Now, we will compare the results obtained from these simulations.

3.2.1 Change of radius of gyration induced by salt presence

Linear chain architecture

We observed that the introduction of salt into the solution did not result in any significant changes in R_g^2 for the linear chains. Numerically, there was a slight decrease, indicating a potential wrapping of ionized PAA segments around the salt ions. However, due to the nature of the data and its standard deviation, it is not possible to confirm this effect conclusively.

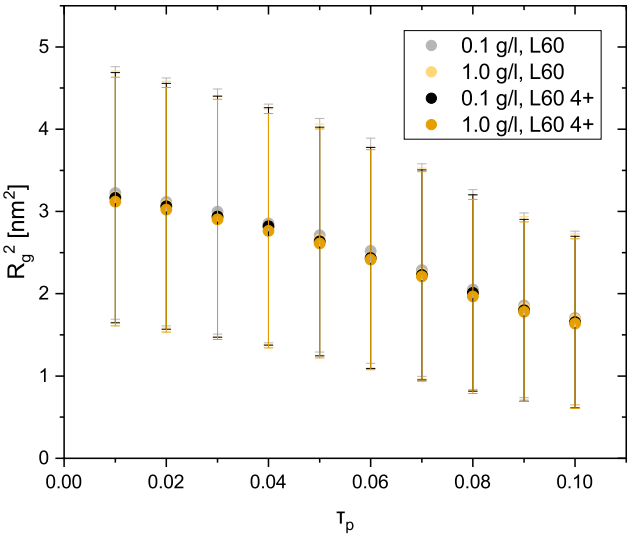

Figure 3.11: R_g^2 in relation to increasing τ_p parameter at $pK_A = 4.5$. L60 denotes linear chains consisting of 60 beads. Transparent colors represent results presented in figure 3.1 and are used as controls. Full colors represent simulations with salt. In yellow is concentration of 1.0 g/l and in black is concentration of 0.1 g/l.

The simulations with a lowered pK_A value yielded similar results. Although we still observed a higher overall R_g^2, there were no significant changes observed upon introducing salt into the solution.

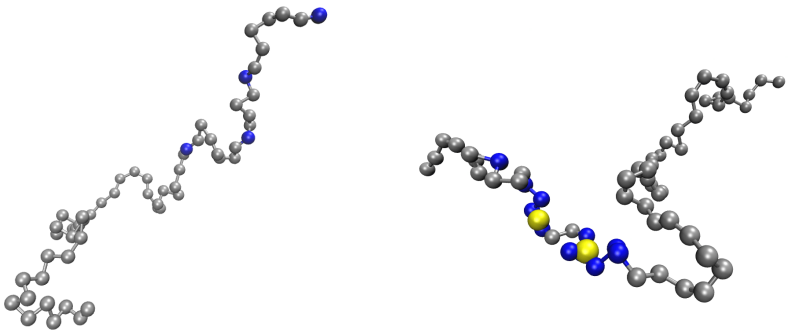

(a) (b)

Figure 3.12: Snapshots of linear chains at $pK_{\mathrm{A}} = 4.5$ and $\tau_p = 0.01$ (a) no salt (b) 10^{-6}M salt content

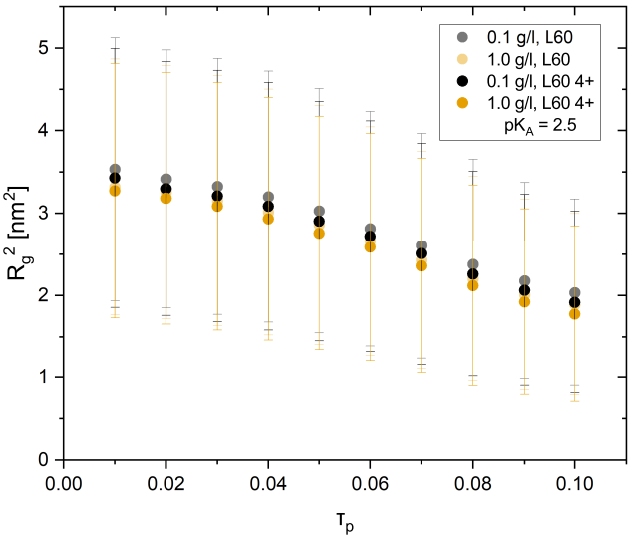

Figure 3.13: $\mathrm{R_g^2}$ in relation to increasing τ_p parameter at $pK_{\mathrm{A}} = 2.5$. L60 denotes linear chains consisting of 60 beads. Transparent colors represent results presented in figure 3.1 and are used as controls. Full colors represent simulations with salt. In yellow is concentration of 1.0 g/l and in black is concentration of 0.1 g/l.

Star architecture

The investigation into the star architecture yielded similiar results. There was only a slight decrease in R_g^2 upon introducing salt into the solution. We attribute this mostly to the PAA segments wrapping around the salt.

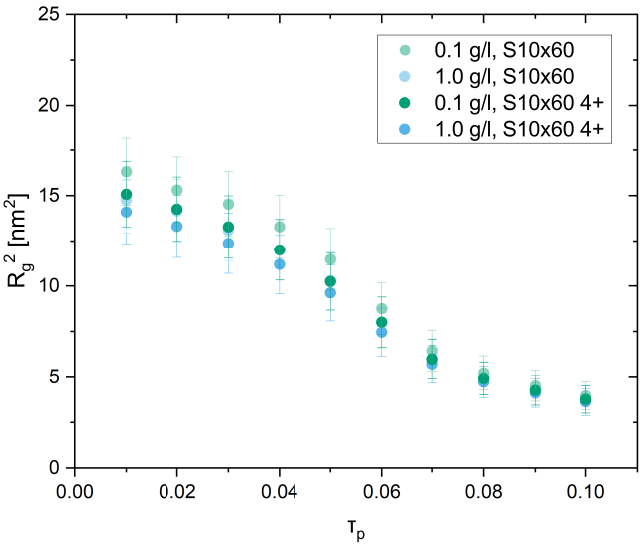

Figure 3.14: R_g^2 in relation to increasing τ_p parameter with $pK_A = 4.5$. S10x60 denotes star architecture consisting of 10 chains with 60 beads each. Transparent colors denote the data depicted in figure 3.5. Full colors represent simulations with salt. In green is concentration of 1.0 g/l and in blue is concentration of 0.1 g/l

Simulations with a lower pK_A value exhibited a similar pattern. Despite the higher degree of ionization, resulting in higher values of R_g^2, there were no significant changes observed in R_g^2 upon introducing salt into the solution. In both cases, the salt ions were incorporated into the star architecture without significantly affecting the conformation of the chain.

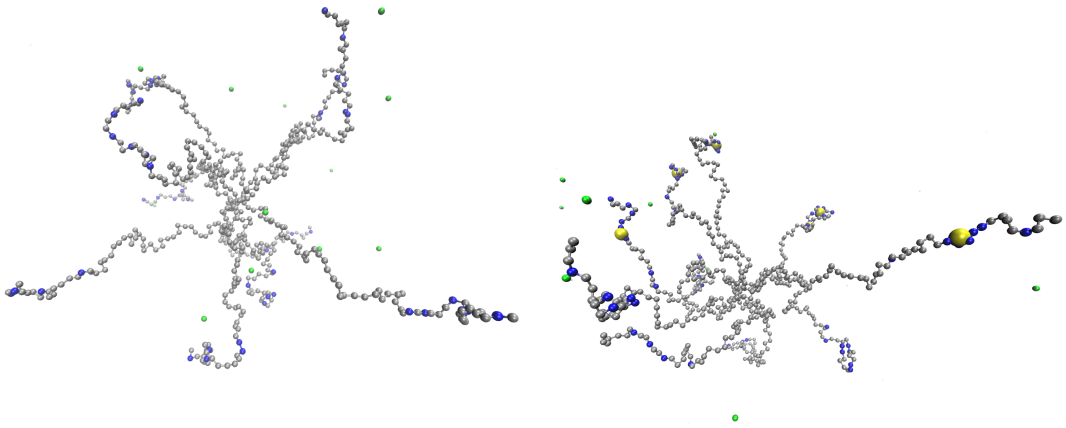

(a) (b)

Figure 3.15: Snapshots of stars at $pK_A = 2.5$ and $\tau_p = 0.01$ (a) no salt (b) 10^{-6} M salt content

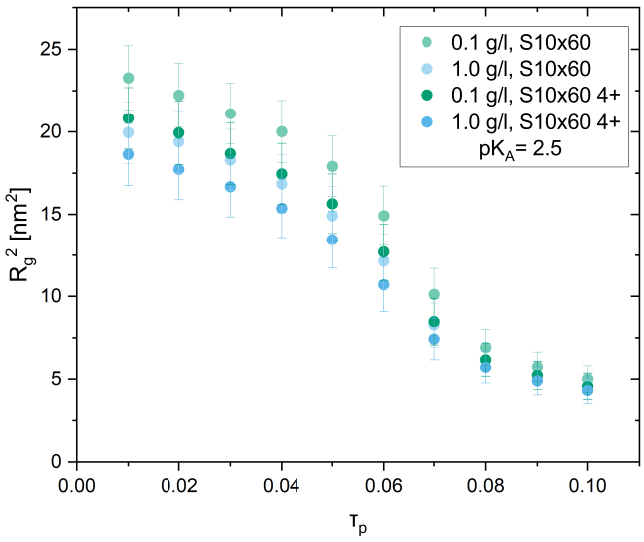

Figure 3.16: R_g^2 in relation to increasing τ_p parameter in basic solution with $pK_A = 2.5$. S10x60 denotes star architecture consisting of 10 chains with 60 beads each. Transparent colors denote the data depicted in figure 3.5. Full colors represent simulations with salt. In green is concentration of 1.0 g/l and in blue is concentration of 0.1 g/l

3.2.2 Change of degree of ionization induced by salt presence

During our investigation, we examined the impact of introducing salt on the degree of ionization. We observed a consistent increase in the overall degree of ionization across all systems. This rise in ionization was attributed to the stabilizing effect of salt ions on the ionized chain, resulting in a reduction in the system's overall energy. These findings were in line with our expectations. Subsequently,

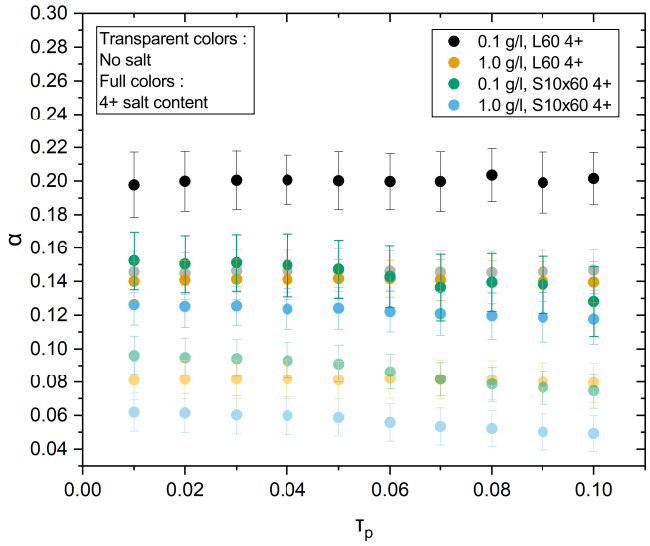

Figure 3.17: Degree of ionization in relation to τ_p parameter at $pK_A = 4.5$. S10x60 denotes star architecture consisting of 10 chains with 60 beads each and L60 denotes linear chains of 60 beads each. Color scheme remains the same as previous plotted data.

we obtained nearly identical results from the system with a decreased pK_A. The degree of ionization showed a consistent increase, similar to the previous systems. This similarity can be attributed to the salt ions still effectively stabilizing the ionized chain, resulting in a reduction in the system's overall energy. These findings were consistent with our earlier observations.

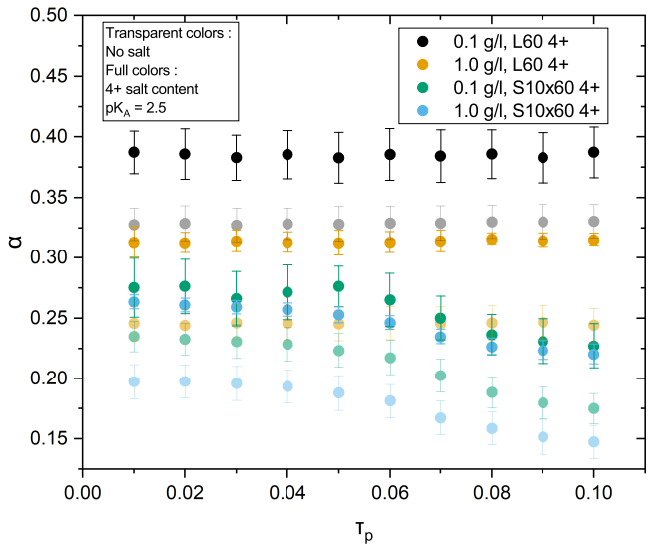

Figure 3.18: Degree of ionization in relation to τ_p parameter at $pK_\mathrm{A} = 2.5$. S10x60 denotes star architecture consisting of 10 chains with 60 beads each and L60 denotes linear chains of 60 beads each. Color scheme remains the same as previous plotted data.

3.3 Polymer clusters approximations

The main prediction from the simulation of the star architecture PAA-PNIPAm is the formation of a hydrophobic core at high values of τ_p, which corresponds to an increase in temperature. However, in this particular case, the polymer chains are connected at the center bead, and breaking this bond is not allowed in the simulation. It is expected that linear chains would behave similarly, but this is highly unlikely. At concentrations of 1.0 g/l and 0.1 g/l, it is statistically improbable for a core consisting of more than two chains to form, as the simulated chains tend to separate from each other due to the amphiphilic nature of the chain.

To acknowledge the limitations of our simulations, we conducted a separate simulation set with the aim of approximating the behavior of linear chains in clusters. In solution, the polymer is not uniformly distributed but can form clusters. In these cluster formations, concentration calculations no longer provide meaningful results. We approximated the clustering of polymer chains by simulating linear polymer chains at concentrations of 64 g/l, 100 g/l, and 200 g/l. These simulations were carried out at a τ_p value of 0.1 to simulate a highly hydrophobic environment, which we associate with high temperature. These simulations were carried out with salt content of 10^{-6} M. We then qualitatively assessed the tendencies displayed by the system.
In all of our simulations, we noticed the emergence of sizable hydrophobic cores, mirroring the behavior observed in star architectures. To illustrate this, a comparison between the pre-simulation and post-simulation states is depicted in figure 3.19. As the concentration increased, the cores exhibited a noticeable growth,

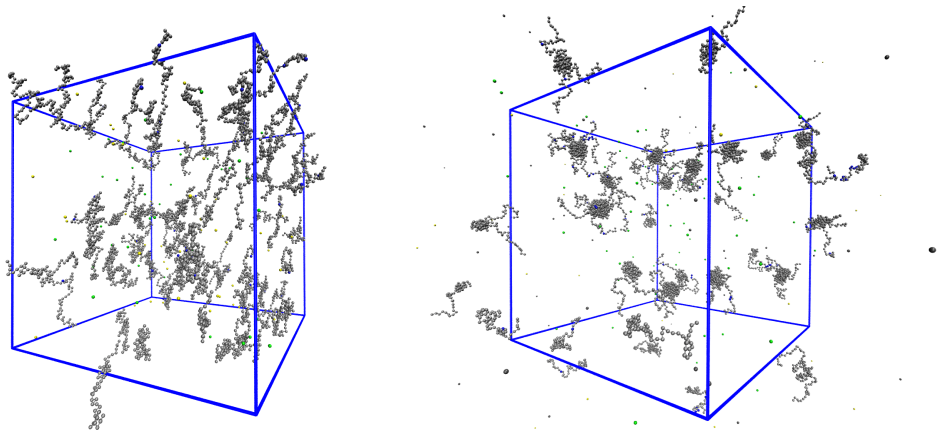

(a) (b)

Figure 3.19: Snapshots of simulations approximating cluster behaviour at $pK_A = 4.5$ and $\tau_p = 0.1$ and concentration of 64 g/l (a) before simulation (b) after simulation

frequently intertwining with each other. This phenomenon can be approximated as a phase transition from a dissolved state to a solid state.

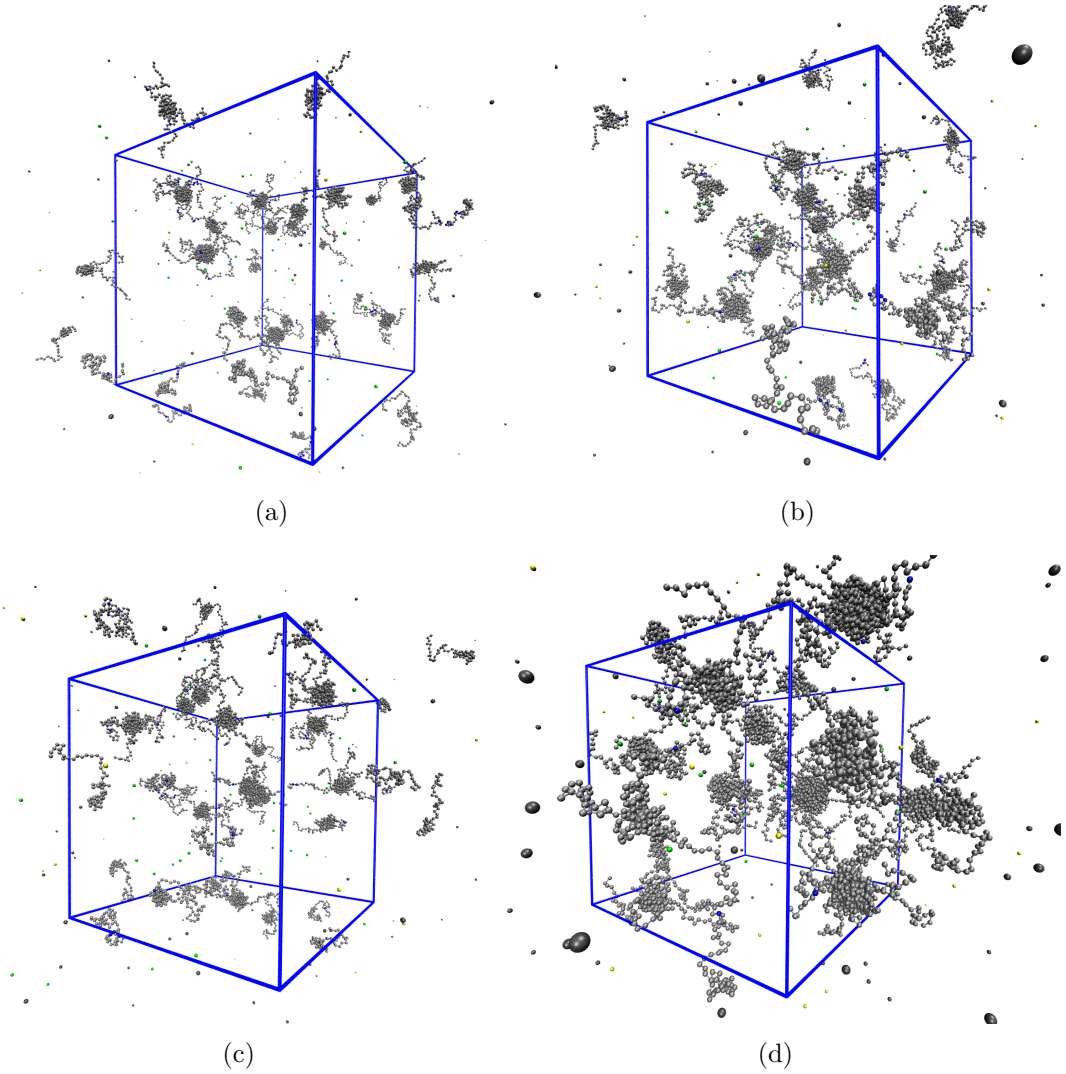

Figure 3.20: Snapshots of simulations approximating cluster behaviour at $pK_{\mathrm{A}} = 4.5$ and $\tau_p = 0.1$ (a) 64 g/l (b) 100 g/l (c) 200 g/l (d) 500 g/l

3.3.1 Cryo STEM

We conducted cryo STEM imaging on specimen of PAA-PNIPAm in a sodium hydroxide solution. The specimens were prepared at different temperatures while maintaining the same concentration of 1.0 g/l. The first specimen was prepared at 25 °C, while the second specimen was prepared at 50 °C. Before the specimen preparation each sample was visually investigated. While specimen kept at 25 °C was a clear solution, the specimen after heating at 50 °C was visually less transparent, and can be described as slightly cloudy. To prepare the specimens, we used a cryo plunging method. Mist chamber was kept at 25°C with a relative humidity of 98%. A small drop of the solution was applied to a copper grid mounted on the tweezer placed in the chamber. Afterward, each specimen was automatically blotted five times on each side of the grid using filtration paper. Following the blotting process, the samples were left undisturbed for approximately 2 minutes to allow for relaxation and creation of thin water layer. Subsequently, the samples were rapidly plunged into liquid ethane that allowed instant freezing of the specimens. They were then transferred to a cryo station, and then on the cryo holder which had been kept under liquid nitrogen. The dewar of the cryo holder was continuously kept refilled with liquid nitrogen to sustain operating temperature below -175 °C. The samples were kept at a low temperature by submerging them in liquid nitrogen throughout the process until the holder was inserted into the microscope. Finally, both specimens were imaged using STEM, and the results were analyzed by measuring the size of representative number of particles and generating the size distributions histograms. Upon visual investigation we found small clusters of our sample forming at temperature of 25 °C. Contrary, sample plunged at 50 °C was found to form large aggregates throughout specimen. Comparison of representative STEM images obtained for these structures is presented in figure 3.21. Then, using obtained images we measured the size of imaged particles and plotted it as a size distributions graphs of particles at two different temperatures for comparison. Size distributions histograms are presented in figure 3.22.

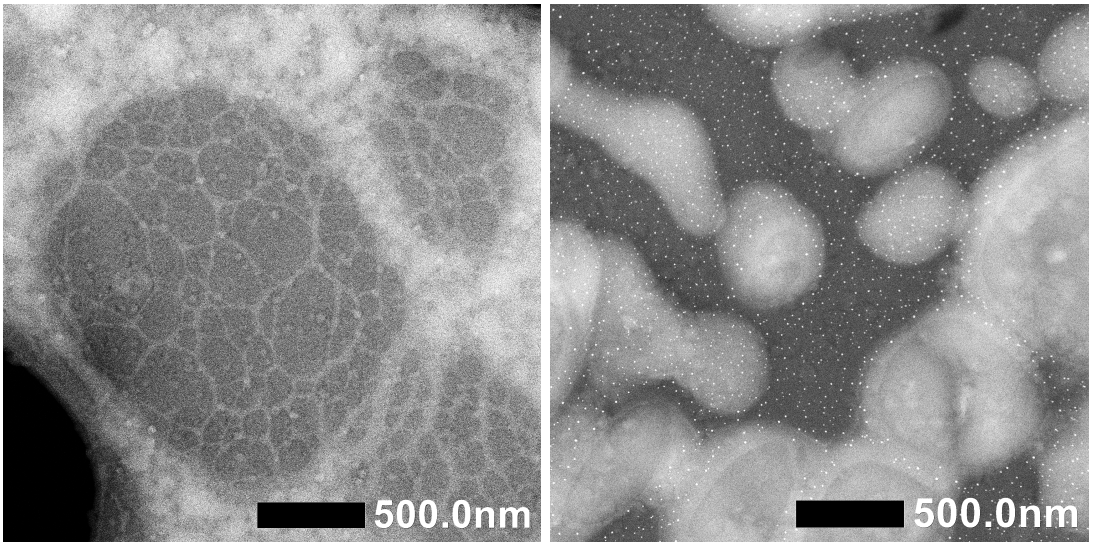

(a) (b)

Figure 3.21: Images recorded with cryo STEM imaging. (a) sample at 25 °C (b) sample at 50 °C

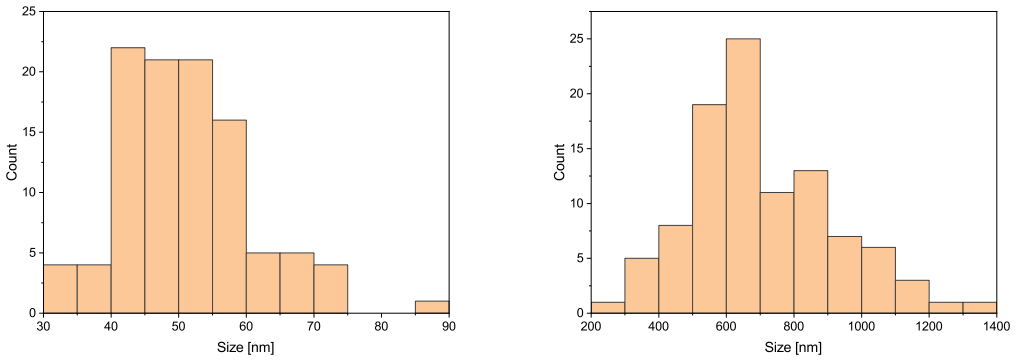

(a) (b)

Figure 3.22: Size distribution of structures observed in PAA-PNIPAm sample in solution of sodium hydroxide (a) sample at 25 °C (b) sample at 50 °C

4. Study limitations and future perspectives

We will now present our view on limitations of this study and possible future perspectives.

Approximating the polymer chain

It is important to note that in our simulation, we focused on copolymer chains comprising 60 beads with a PAA/PNIPAM ratio of 0.4/0.6. While the block ratio is based on real observations, the chosen chain length is arbitrary. Although a 60-monomer chain can be considered a polymer in its essence, this may impose limitations on fully exploring the behavior of these chains. For future investigations, it would be advantageous to simulate copolymer chains of various lengths to gain a more comprehensive understanding of their properties.

Varying the solution pH

Although not the primary objective of our study, we observed that adjusting the pK_{A} of the PAA segments, as an approximation of different solvent pH levels, resulted in an increase in the size of the simulated chains. These findings raise intriguing questions about the potential outcomes when exploring a wider range of pK_{A} values. We believe that conducting studies over a broader spectrum of pK_{A} would greatly contribute to a deeper understanding of the intricacies within this system.

Star architectures

Our investigation focused on star architecture PAA-PNIPAm chains, employing a model comprising 10 copolymer chains, each consisting of 60 beads. This model was chosen for it's relative computational cheapness and because the real association number is unknown. While this model provides a reasonable approximation of a micelle structure, we recognize the potential to enhance our understanding of the system by exploring variations in these architectures and studying the trends observed.

Approximating polymer clusters

We conducted a study on polymer systems in rather extreme concentrations as an approximation of polymer clusters in solution. We simulated this in solvent at τ_p value of 0.1 which approximates solution at high temperature. This confirmed the ability of linear chains to form dense hydrophobic cores. However by simulating over the whole range of τ_p as was done with other simulations, we could explore this behaviour more closely. While these simulations have proven themselves to be computationally difficult, we believe that future research could possibly yield interesting results.

Cryo imaging

In our Cryo-STEM imaging of PAA-PNIPAm in a sodium hydroxide solution, we primarily focused on temperature as the parameter of interest. However, to deepen our understanding of this system, further investigation by varying these parameters is needed. We propose conducting imaging experiments that compare the differences observed when altering the concentration of the sample and the pH level. Additionally, we suggest exploring the system's temperature dependence in a more precise manner. These proposed variations in parameters have the potential to provide valuable insights into the behavior of the polymer system.

Conclusion

We conducted as study on stimuli responsive copolymer system of poly(acrylic acid-block-N-isopropylacrylamide) in solution. Theorethical study was done using hamiltonian Monte Carlo simulations in reaction ensamble. We used coarse grained model for our simulations using two distinct architectures one being linear chains and the second being polymer stars. We investigated the effect of varying concentration of the polymer(0.1 g/l and 1.0 g/l) and presence of meso-tetrakis(N-methyl-4-pyridyl)porphine tetrakis(p-toluenesulfonate) as well as varying τ_p parameter in range from 0.01 to 0.1 as an approximation of temperature change. We then investigated effects of these stimuli on mean value of R_g^2 and degree of ionization. In the simulations investigating the effect of concentration we found no significant difference in mean values of R_g^2 between the two concentrations in both architectures. We observed sharp decrease in mean value of R_g^2 with increase of τ_p parameter. This was in line with our expectations that stemmed from experimental data in current literature, from which we draw the conclusion that observed decrease in size was corresponding to the phase transition that the polymer undergoes when exposed to temperatures above 32 °C. We observed higher degree of ionization in simulations conducted at lower concentration of polymer (0.1 g/l) which is in line with current understanding of acid dissociation. We failed to see any statistically significant change in mean value of R_g^2 upon introducing salt into the system in both polymer architectures. We attribute this to the fact that studied salt is multivalent (4^+) and therefore the effect of increased ionization that would ultimately lead to stretching of the polymer chain is diminished by conformation of the chain around the salt particle as opposed to monovalent salt, where we would expect overall increase in size. We observed an increase in overall degree of ionization upon introduction of salt, which was in line with our expectations.

Knowing these insights, we proposed simulations reflecting the real specimen studied by cryo-STEM. It was performed by the replication of the exact same simulation set with change of the pK_A value to 2.5. In this way we reached the approximation of basic solution. As expected this lead to higher degree of ionization, however we also observed relatively large increase in mean values of R_g^2. We explain this as stretching of highly ionized chains. Same as with previous simulation we saw no statistically significant changes in size upon changing concentration of the polymer or presence of salt. Additionally we conducted simulations approximating polymer clusters in solution at high temperature, where we observed formation of large hydrophobic core, which sizes rose with the concentration. This was in line with the observations of cryo-STEM imaging, where we compared a sample of the polymer in solution of sodium hydroxide at 25 °C and consequently at 50°C. At lower temperature we observed formations of small clusters ranging from 30 nm to 90 nm, with the most common sizes being in range from 40 - 60 nm. At higher temperature we observed formation of large aggregates of the polymer with size ranging from 200 nm to 1400 nm, with the most common sizes being 500-700 nm. This was in line with what experimental data acquired by dynamic light scattering predicted.

Bibliography

[1] Solmaz Saghebasl, Abolfazl Akbarzadeh, Armita Mahdavi Gorabi, Nasrin Nikzamir, Mirabdullah Seyed Sadjadi, and Ebrahim Mostafavi. Biodegradable functional macromolecules as promising scaffolds for cardiac tissue engineering. *Polymers for Advanced Technologies*, 33(7):2044–2068, 2022.

[2] Luboš Běhálek. Struktura polymerů a její vliv na vlastnosti, 2015.

[3] *Models of Polymer Chains*, chapter 1, pages 1–67. John Wiley Sons, Ltd, 2002.

[4] George M. Whitesides and Bartosz Grzybowski. Self-assembly at all scales. *Science*, 295(5564):2418–2421, 2002.

[5] Lucie Nová, Filip Uhlík, and Peter Košovan. Local ph and effective pka of weak polyelectrolytes – insights from computer simulations. *Phys. Chem. Chem. Phys.*, 19:14376–14387, 2017.

[6] Margarita A. Dyakonova, Anatoly V. Berezkin, Konstantinos Kyriakos, Sandra Gkermpoura, Maria T. Popescu, Sergey K. Filippov, Petr Štěpánek, Zhenyu Di, Constantinos Tsitsilianis, and Christine M. Papadakis. Salt-induced changes in triblock polyampholyte hydrogels: Computer simulations and rheological, structural, and dynamic characterization. *Macromolecules*, 48(22):8177–8189, 2015.

[7] Xinqiao Jia and Kristi L. Kiick. Hybrid multicomponent hydrogels for tissue engineering. *Macromolecular Bioscience*, 9(2):140–156, 2008.

[8] N Peppas. Hydrogels in pharmaceutical formulations. *European Journal of Pharmaceutics and Biopharmaceutics*, 50(1):27–46, 2000.

[9] Mark Rubinstein and Ralph H. Colby. *Polymer physics*. Oxford University Press, 2003.

[10] Pierre-Gilles de Gennes. *Scaling concepts in polymer physics*. Cornell Univ. Press, 2005.

[11] G Ali Mansoori. Flory-huggins theory of polymer solutions and its improvement, 11 2021.

[12] A. Hemsley and Nina Gabarayeva. Exine development: The importance of looking through a colloid chemistry "window". *Plant Systematics and Evolution*, 263:25–49, 12 2007.

[13] Linda E. Franken, Egbert J. Boekema, and Marc C. Stuart. Transmission electron microscopy as a tool for the characterization of soft materials: Application and interpretation. *Advanced Science*, 4(5):1600476, 2017.

[14] John Watt, Dale L. Huber, and Phoebe L. Stewart. Soft matter and nanomaterials characterization by cryogenic transmission electron microscopy. *MRS Bulletin*, 44(12):942–948, 2019.

[15] R. Henderson, J.M. Baldwin, T.A. Ceska, F. Zemlin, E. Beckmann, and K.H. Downing. Model for the structure of bacteriorhodopsin based on high-resolution electron cryo-microscopy. *Journal of Molecular Biology*, 213(4):899–929, 1990.

[16] D Danino, A Bernheim-Groswasser, and Y Talmon. Digital cryogenic transmission electron microscopy: an advanced tool for direct imaging of complex fluids. *Colloids and Surfaces A: Physicochemical and Engineering Aspects*, 183-185:113–122, 2001.

[17] Dganit Danino. Cryo-tem of soft molecular assemblies. *Current Opinion in Colloid & Interface Science*, 17(6):316–329, 2012.

[18] Jose Callejas-Fernandez, Jhon Ramos, Oihane Sanz, Jacqueline Forcada, J.L. Ortega-Vinuesa, Alberto Martin-Molina, Miguel A. Rodríguez-Valverde, Maria Tirado-Miranda, Artur Schmitt, B. Sierra-Martin, A. Maldonadovaldivia, Antonio Fernández-Barbero, Ramon Pons, Luis Fermin Capitan-Vallvey, Alfonso Salinas-Castillo, Alejandro Lapresta-Fernández, Blanca Vazquez, Maria Rosa Aguilar, and Julio San Roman. *Experimental techniques used for the characterization of soft nanoparticles*, volume 2014, pages 19–108. 01 2014.

[19] Stephen J. Pennycook. Transmission electron microscopy: A textbook for materials science, second edition. springer, new york, 2009, 932 pages. isbn 978-0-387-76500-6 (hardcover), isbn 978-0-387-76502-0 (softcover). *Microscopy and Microanalysis*, 16(1):111–111, 2010.

[20] Richard Chudoba, Jan Heyda, and Joachim Dzubiella. Temperature-dependent implicit-solvent model of polyethylene glycol in aqueous solution. *Journal of Chemical Theory and Computation*, 13(12):6317–6327, 2017. PMID: 29032685.

[21] Sebastian Kmiecik, Dominik Gront, Michal Kolinski, Lukasz Wieteska, Aleksandra Elzbieta Dawid, and Andrzej Kolinski. Coarse-grained protein models and their applications. *Chemical Reviews*, 116(14):7898–7936, 2016. PMID: 27333362.

[22] Soumil Y. Joshi and Sanket A. Deshmukh. A review of advancements in coarse-grained molecular dynamics simulations. *Molecular Simulation*, 47(10-11):786–803, 2021.

[23] Peter Bonate. A brief introduction to monte carlo simulation. *Clinical pharmacokinetics*, 40:15–22, 02 2001.

[24] Jiří Kolafa. *Molekulové modelování a simulace*. Ústav Fyzikální chemie, VŠCHT, 2021.

[25] Daan Frenkel and Berend Smit. *Understanding molecular simulation: From algorithms to applications*. Academic Press, 2012.

[26] Nicholas Metropolis and S. Ulam. The monte carlo method. *Journal of the American Statistical Association*, 44(247):335–341, 1949.

[27] A. Irbäck. Hybrid Monte Carlo simulation of polymer chains. *The Journal of Chemical Physics*, 101(2):1661–1667, 07 1994.

[28] W. R. Smith and B. Triska. The reaction ensemble method for the computer simulation of chemical and phase equilibria. i. theory and basic examples. *The Journal of Chemical Physics*, 100(4):3019–3027, 1994.

[29] Lucie Nová, Filip Uhlík, and Peter Košovan. Local ph and effective pka of weak polyelectrolytes – insights from computer simulations. *Phys. Chem. Chem. Phys.*, 19:14376–14387, 2017.

[30] Filip Uhlík, Peter Košovan, Ekaterina B. Zhulina, and Oleg V. Borisov. Charge-controlled nano-structuring in partially collapsed star-shaped macromolecules. *Soft Matter*, 12:4846–4852, 2016.

[31] P. P. Ewald. Die berechnung optischer und elektrostatischer gitterpotentiale. *Annalen der Physik*, 369(3):253–287, 1921.

[32] Anastasiia Fanova, Miroslav Štěpánek. Unpublished results.

[33] Chao Zhou, Shanshan Qian, Xia-jun Li, Fang Yao, John Forsythe, and Guo-Dong Fu. Synthesis and characterization of well-defined paa-peg multiresponsive hydrogels by atrp and click chemistry. *RSC Adv.*, 4, 10 2014.

[34] Filip Uhlík, Peter Košovan, Zuzana Limpouchová, Karel Procházka, Oleg V. Borisov, and Frans A. M. Leermakers. Modeling of ionization and conformations of starlike weak polyelectrolytes. *Macromolecules*, 47(12):4004–4016, 2014.

[35] Wolfhard Janke. Statistical analysis of simulations:data correlations and error estimation. 08 2009.

Attachments

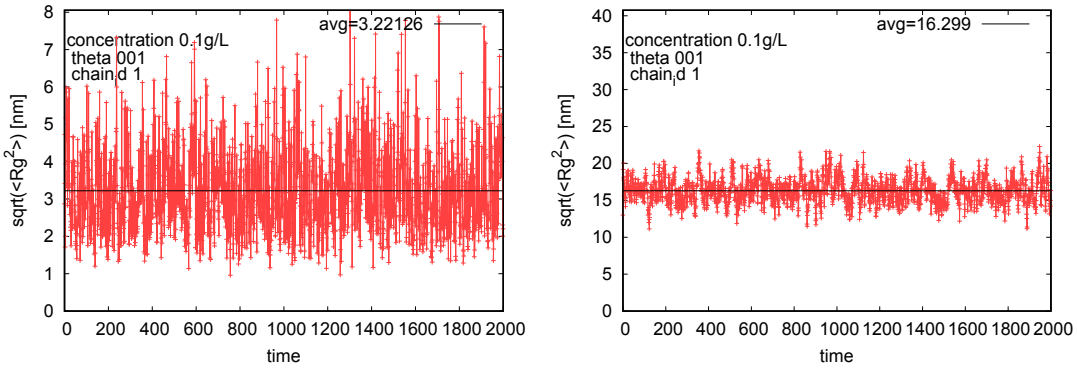

(a) (b)

Figure 4.1: Time evolution of Rg. (a) Rg time evolution of chains (b) Rg time evolution of stars